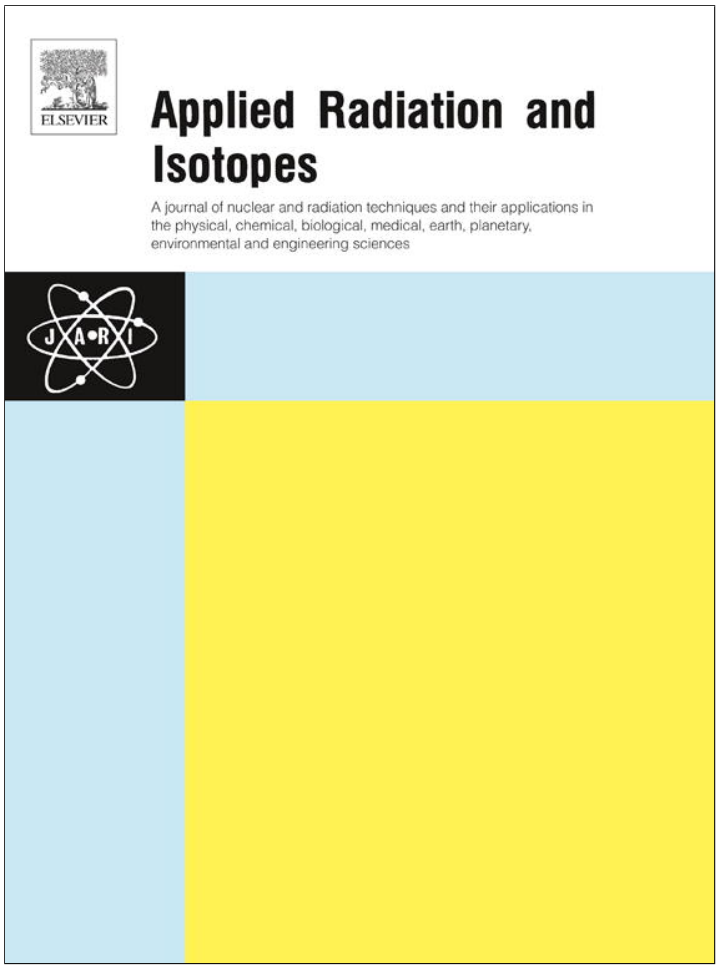

(This is a sample cover image for this issue. The actual cover is not yet available at this time.)

Applied Radiation and Isotopes 70 (2012) 1485–1493

Contents lists available at SciVerse ScienceDirect

Applied Radiation and Isotopes

journal homepage: www.elsevier.com/locate/apradiso

Benchmarking the GEANT4 full system simulation of an associated alpha-particle detector for use in a D–T neutron generator ☆

Xiaodong Zhang [a,*], Jason P. Hayward [a,b], Joshua W. Cates [a], Paul A. Hausladen [b,a], Mitchell A. Laubach [a], Johnathan E. Sparger [a], Samuel B. Donnald [a]

[a] Department of Nuclear Engineering, University of Tennessee, TN 37996, USA
[b] Oak Ridge National Laboratory, Oak Ridge, TN 37831, USA

HIGHLIGHTS

- GEANT4-based full system model of an associated alpha-particle detector.
- Study the influence of different-sized fiber-optic faceplate on position performance.
- Study the influence of optical grease to its position performance.
- Less than 1 mm position uncertainty is expected for associated alpha-particle detector.
- Study the influence of background radiations inside a D–T generator.

ARTICLE INFO

Article history:
Received 21 October 2011
Received in revised form
18 April 2012
Accepted 25 April 2012
Available online 2 May 2012

Keywords:
Fast neutron imaging
Associated alpha-particle detector
YAP:Ce
GEANT4

ABSTRACT

The position-sensitive alpha-particle detector used to provide the starting time and initial direction of D–T neutrons in a fast-neutron imaging system was simulated with a GEANT4-based Monte Carlo program. The whole detector system, which consists of a YAP:Ce scintillator, a fiber-optic faceplate, a light guide, and a position-sensitive photo-multiplier tube (PSPMT), was modeled, starting with incident D–T alphas. The scintillation photons, whose starting time follows the distribution of a scintillation decay curve, were produced and emitted uniformly into a solid angle of 4π along the track segments of the alpha and its secondaries. Through tracking all photons and taking into account the quantum efficiency of the photocathode, the number of photoelectrons and their time and position distributions were obtained. Using a four-corner data reconstruction formula, the flood images of the alpha detector with and without optical grease between the YAP scintillator and the fiber-optic faceplate were obtained, which show agreement with the experimental results. The reconstructed position uncertainties of incident alpha particles for both cases are 1.198 mm and 0.998 mm respectively across the sensitive area of the detector. Simulation results also show that comparing with other faceplates composed of 500 μm, 300 μm, and 100 μm fibers, the 10-μm-fiber faceplate is the best choice to build the detector for better position performance. In addition, the study of the background originating inside the D–T generator suggests that for 500-μm-thick YAP:Ce coated with 1-μm-thick aluminum, and very good signal-to-noise ratio can be expected through application of a simple threshold.

1. Introduction

The associated alpha-particle technique is widely used in a fast neutron imaging system based on a Deuterium–Tritium (D–T) generator, especially for interrogating the Special Nuclear Materials (SNM) (Hausladen et al., 2005, 2007; Perot et al., 2007, 2009; Nebbia et al., 2005). In a D–T generator, a 3.5-MeV alpha particle and a 14-MeV neutron are produced back-to-back via the D+T reaction. By detecting the time and position of alphas, and furthermore combining with the beam position on the D–T target, the starting time and initial direction of neutrons can be obtained. To achieve a high quality image of interrogated SNM in a fast neutron imaging system, the associated alpha-particle detector must have very high timing and spatial resolution. For fulfilling these demands, two kinds of very promising scintillation

☆This material is based upon work supported by the U.S. Department of Homeland Security under Grant Award Number 2010-DN-077-ARI044-02.
* Corresponding author. Tel.: +1 865 974 2506.
E-mail address: xzhang39@utk.edu (X. Zhang).

0969-8043/$ - see front matter © 2012 Elsevier Ltd. All rights reserved.
http://dx.doi.org/10.1016/j.apradiso.2012.04.026

detectors based on cerium-doped yttrium aluminum perovskite (YAP:Ce) (Pesente et al., 2007) and gallium-doped zinc oxide (ZnO:Ga) (Neal et al., 2008; Hausladen et al., 2005; Cooper et al., 2003) were proposed and studied in recent years. Compared with the ZnO:Ga (Bourret-Courchesne et al., 2009) scintillator, the YAP:Ce (Moszynski et al., 1997) scintillator is brighter. Its light yield is about 18,000 photons/MeV for gammas, while the light yield of ZnO:Ga is only about 9700 photons/MeV for gammas. However, considering the decay time of the two materials, ZnO:Ga is faster than YAP:Ce, 800 ps vs. 26 ns (90%)+67 ns (10%). The latter is considered as a candidate of the next generation associated alpha-particle detector because of its very short decay time.

In this paper, we only concentrate our discussion on a position-sensitive YAP:Ce-based alpha-particle detector. Here, the YAP:Ce was chosen to build the associated alpha-particle detector. The main consideration is that the large light yield is helpful to improve the signal-to-noise ratio of the detector. In addition, it is also helpful to improve the detector's timing performance (Cates et al., 2011). Some other considerations in the choice of YAP:Ce include (1) large diameter monolithic crystal sizes are available; (2) the crystal can withstand the thermal stress of the fabrication process; and (3) the decay time of scintillator is fast enough to make the detector able to detect the associated alphas without an observable overlap of signals (see Fig. 2) for a 4π neutron output of 10^8 per second.

In order to benchmark this design (see Fig. 1), a Monte Carlo simulation program in the framework of GEANT4 (Agostinelli et al., 2003) was developed. With this program, the whole detector, which consists of a YAP:Ce scintillator, a fiber-optic faceplate, a light guide, and a PSPMT, was modeled. Whole modeling of the detector makes us possible to study its time and position performance. One main challenge of this work is the simulation of fiber-optic faceplate consisting of very small-size (down to $10 \times 10\ \mu m^2$) fibers, which make the program run very slowly (about 10 s per event on a computer with two Quad-Core 2.93 GHz Intel® Xeon® processors and 16 GB of random-access memory (RAM)). In Blackston's paper (Blackston et al., 2008), the purpose of the simulation was to design of the light guide. So, the program only started from the light guide, and no fiber faceplate and YAP:Ce were simulated. In this way, the scintillation photons transported outside the fiber were not taken into account.

With the model of whole detector in the current program, the influence of these photons to the performance of the detector, for instance, flood field response, was studied. Furthermore, the best matched fiber size of faceplate for the current design of the light guide was also studied and optimized. In addition, the interface between the YAP:Ce scintillator and fiber faceplate with and without grease as well as directly coupled, the propagation of scintillation photons, light collection efficiency, flood field response, and position uncertainty of the detector were also studied. Additionally, the influence of background radiations originating inside the D–T generator was studied as well.

2. Detector structure and modeling

2.1. Detector structure

The associated alpha-particle detector (see Fig. 1) consists of a YAP:Ce scintillator (Baccaro et al., 1995, 1998; Derenzo et al., 2000; Zorenko et al., 2007), a fiber-optic faceplate, a light guide, and a position-sensitive photo-multiplier tube (PSPMT-Hamamatsu H8 500). In this design, a 500-μm-thick single crystal, YAP:Ce, is used to convert the energy deposited by the alpha particle into scintillation light. Based on the GEANT4 simulation, the range of 3.5-MeV alphas in YAP is about 7.09 ± 0.09 μm. So, this thickness is enough to stop them. Additionally, aluminum of 1 μm is deposited on the top of the scintillator, which is able to eliminate the influence of other

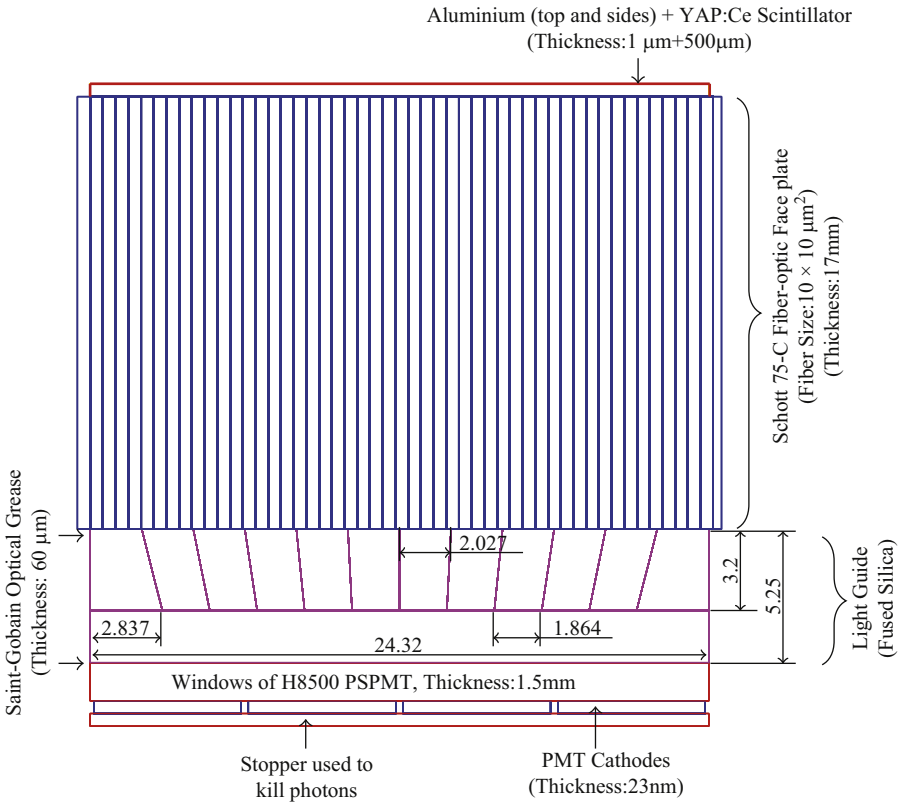

Fig. 1. Schematic of the associated alpha-particle detector.

background radiations, such as deuterons, tritons, and secondary electrons (for details, see Section 3.1). This very thin layer of aluminum also serves as an electrical ground path to prevent charge buildup on the scintillator (Chichester et al., 2005). For the 3.5-MeV alphas, the energy loss in the aluminum film is only about 195 ± 10 keV. Such small energy loss will not produce any significant difference in performance for detecting alphas.

In order to improve the light collection efficiency, optical grease (Saint-Gobain BC-630) modeled as 60 μm thick is used at the interfaces between the faceplate and light guide as well as the light guide and PSPMT in the simulation. No optical grease can be used at the interface between the YAP:Ce and fiber faceplate because it does not survive the bake-out process used in the fabrication of the D–T generator. In the bake-out process, the D–T generator is heated to 350 °C for up to one week. However, in order to study how large its influence will be in the performance of the detector, both cases, with and without optical grease between the YAP and fiber faceplate, were simulated and compared with the experimental results (see Sections 3.2 and 3.3 for details). For the with-grease case, the thickness of grease is 60 μm; for the without-grease case, a 1-μm vacuum gap is used.

A 17-mm-thick Schott 75C fiber-optic faceplate with optical numerical aperture of 0.58 is used. The reasons to use the fiber faceplate are two in number: (1) in order to guide and collimate the scintillation photons through the vacuum interface, i.e., the wall of the generator and (2) to limit the divergence of scintillation light in transit so that the position resolution of the detector is not degraded. Four different sizes of fiber faceplate which are made of 10 μm, 100 μm, 300 μm, and 500 μm optical fibers respectively were simulated. The simulation results show that the faceplate composed of 10-μm fibers is the best one for the current design (see Section 3.3 for details).

The segmented light guide (see Fig. 1) used in the detector consists of 12×12 trapezoidal pixels whose dimensions are given in Fig. 1. Its optimization and tapered design are discussed in Blackston's work (Blackston et al., 2008). The bottom part of the light guide and the window of the PSPMT are used to diffuse the scintillation photons more uniformly onto the readout pixels of the PSPMT. In the program, only four by four pixels at the center of the PSPMT were modeled, which is consistent with the readout board that was developed for testing our detector. The modeling of photocathode is discussed in Section 2.2. Additionally, in order to accelerate the speed of the program, a stopper (see Fig. 1) was added under the photocathode of the PSPMT, which is used to kill the photons after they pass over the photocathode.

2.2. Detector optical model

In the Monte Carlo simulation program, the whole detector system (see Fig. 1) described in Section 2.1 was modeled. The basic properties of materials used to assemble the detector are listed in Table 1.

To simulate the whole process of detection for alpha particles, the physics list included low energy electromagnetic physics as well as scintillation and transportation of optical photons. For the simulation of optical boundary processes, the GLISUR model (Agostinelli et al., 2003) was used. With this model, the complex indexes of refraction of metals, such as bialkali photocathode and aluminum reflector (see Table 2), were used to calculate the absorption and reflection of photons at the dielectric–metal boundary interfaces. In the program, the interfaces between the YAP:Ce and aluminum film, light guide pixels and aluminum reflector as well as the PMT window and photocathode were modeled with the dielectric–metal interfaces. For the other materials, such as the YAP:Ce, the fiber faceplate, the light guide, and the PMT windows, the refractive indexes and absorption length as a function of wavelength (see Tables 3 and 4) were used. The boundaries between them were modeled with dielectric–dielectric interfaces. Since the surfaces of all materials used to build the detector are highly polished, their surface finish was set as polished.

In order to more precisely simulate the scintillation process of YAP:Ce, some other optical properties of YAP:Ce (see Table 4), such as absorption length and the fast and slow components of scintillation, were also used. Because there are no built-in functions to precisely define the fast and slow components of the scintillation photon distributions as a function of wavelength in GEANT version 4.9.4.p01 (only two arrays with separated values are used), it is difficult to reproduce these distributions very precisely. For best results, a very small step, 10 nm, was used to model the fast and slow components of scintillation (see Table 4). With such fine steps, the wavelength distribution of scintillation photons in the simulation is almost the same as the experimental result described in Zorenko et al. (2007). Due to the finite number of these arrays in GEANT4, it is still not as smooth as one would expect for experimental data.

In addition, the intrinsic energy resolution of YAP:Ce is 1.3% (Kapusta et al., 1999). Its Birks' constant for alphas is 0.0163 mm/MeV, which is calculated with the factory specification of

Table 2
Refractive indexes of aluminum reflector (Rakic, 1995) and bialkali photocathode (Motta and Schnert, 2005) as well as the quantum efficiency of photocathode.

Aluminum reflector			Bialkali photocathode			
Wavelength (nm)	Refractive index		Wavelength (nm)	Refractive index		Quantum efficiency[a] (%)
	Real	Imaginary		Real	Imaginary	
248	0.18	2.90	–	–	–	–
310	0.28	3.71	380	1.92	1.69	26.4
326	0.31	3.92	395	2.18	1.69	25.8
365	0.40	4.40	410	2.38	1.71	24.6
413	0.52	5.00	425	2.61	1.53	23.4
443	0.61	5.37	440	2.70	1.50	21.8
477	0.73	5.78	455	2.87	1.44	20.0

[a] Taken from the data sheet of Hamamatsu PSPMT-H8500.

Table 1
Material properties of alpha-particle detector.

Name	Materials	Density (g/cm^3)	Comments
Reflector	Aluminum	2.702	On the YAP:Ce and between the pixels of lightguide
YAP:Ce	$YAlO_3$:Ce	5.35	Yield: 18/keV; Birks constant: 0.0163 mm/MeV; time (ns): 26(90%)+67(10%)
Fiber faceplate	Schott 75C	3.29	Core percentage: >95%
Light guide	Fused silica	2.203	–
PMT window	Borosilicate	2.23	–
Photocathode	Bialkali	3.2	Sb–K–Cs
Optical grease	$(C_2H_6OSi)_n$	1.06	Saint-Gobian BC-630

Table 3
Refractive indexes and absorption length of fiber faceplate, light guide, and PMT window (taken from the factory specification of materials).

Wavelength (nm)	Fiber core		Fiber clad		Light guide		PMT window		Grease	
	R_{index}	Abs. (mm)	R_{index}	Abs. (mm)	R_{index}	Abs. (mm)	R_{index}	Abs. (mm)	R_{index}	Abs. (mm)
300	1.618	6.4	1.504	6.4	1.488	138.0	1.553	1.8	1.496	195.0
350	1.611	120.0	1.498	120.0	1.477	138.0	1.539	40.9	1.482	195.0
375	1.608	495.0	1.497	495.0	1.473	138.0	1.534	63.1	1.477	195.0
400	1.605	1245.0	1.493	1245.0	1.470	138.0	1.531	85.1	1.473	195.0
450	1.599	1995.0	1.489	1995.0	1.466	138.0	1.525	81.9	1.468	195.0

Table 4
Optical parameters of YAP:Ce (Zorenko et al., 2007; Baccaro et al., 1998).

Photon wavelength (nm)	Refractive index	Absorption length (mm)	Scintillation photon	
			Fast part	Slow part
450	1.915	175	0.0	0.0
440	1.916	176	0.0	0.0
430	1.918	177	0.02	0.0
420	1.919	176	0.03	0.001
410	1.921	175	0.04	0.005
400	1.923	174	0.06	0.014
390	1.926	160	0.1	0.015
380	1.928	150	0.15	0.015
370	1.931	140	0.2	0.015
360	1.934	125	0.15	0.015
350	1.938	100	0.06	0.014
340	1.942	75	0.04	0.005
330	1.946	3	0.03	0.001
320	1.951	0	0.02	0.0
310	1.957	0	0.0	0.0
300	1.963	0	0.0	0.0

beta-over-alpha light yield ratio of 3.8. Since this version of GEANT4 can simulate the rise time of a scintillator, the rise time of 240 ps (Derenzo et al., 2000) for YAP:Ce was also used, which makes us be able to more precisely simulate the time distribution of scintillation photons.

The Monte Carlo program starts by shooting alpha particles at the scintillator. By recording the deposited energy of the alpha particle in the YAP:Ce and taking the scintillation process and properties of YAP:Ce into account, the initial scintillation photons along the tracks of the alpha particle and its secondaries are produced. Due to the mismatch of refractive indexes between the interface of YAP ($R_{index}=1.93$) and vacuum ($R_{index}=1$), most photons produced by the incident alpha particle are reflected back to the scintillator and are finally absorbed in it. Only a small fraction of them within the critical angle can go out the scintillator, pass over the vacuum interface, and then finally get to the faceplate. In the fiber faceplate, these photons are transported in two ways: inside the fiber (here and after, we define the photons transported inside the fiber as collimated photons) and outside the fiber. (Photons are transmitted obliquely inside the faceplate, i.e., they pass through several fibers. Here and after, we define these photons as uncollimated photons.) Due to the limitation of the small numerical aperture (0.58) of the fiber faceplate, most of the uncollimated photons outside the acceptance angle of the detector will be lost. The uncollimated photons inside the acceptance angle of the detector and the collimated photons can pass through the faceplate, light guide, PMT window, and finally reach the photocathode. In addition, the uncollimated photons outside the acceptance angle of the detector can also have a chance reach the photocathode through the multi-scattering process in the faceplate. This will be discussed in detail in Section 3.2.

Due to the small quantum efficiency shown in Table 2, very few photoelectrons are produced (see Table 5 and Fig. 2). In Fig. 2, the very long tails of photon/photoelectron distributions in the plot are mainly caused by the relatively slow decay time (see Table 1) of the scintillator. Additionally, by comparing the two time distributions of photons/photoelectrons in the YAP:Ce and photocathode, it is apparent that the most of the photons produced by incident alpha particle will not reach the photocathode to produce photoelectrons.

3. Simulation and experimental results and discussion

3.1. Response to background radiations

Because this detector will be operated in a neutron generator, it should be insensitive to the background radiations produced in it, such as deuterons, tritons, secondary electrons, neutrons, X-rays and gammas. The elastic scattering of the deuteron and triton beam as well as the sputtering of target atoms will cause the deuteron and triton background. The gammas mainly come from inelastic scattering of fast neutrons with structural materials of the D–T generator. The X-rays are mainly produced through the process of bremsstrahlung and the de-excitation of excited atomic energy levels. Careful considerations in this design have been taken to minimize their influence. To minimize the influence of X-rays, gammas and neutrons, a very thin (500 μm) scintillator is used. A simple threshold is effective for discriminating against background because: (1) the scintillation crystal's efficiency for said background radiations is low, and (2) said background radiations tend to deposit very little energy when they do interact. To stop deuterons, tritons, and secondary electrons, an aluminum film of 1-μm thickness is used.

The secondary electrons with the energy of 2–3 eV have chance to be back accelerated by the accelerating high voltage, say −100 kV. Part of them can escape from the suppressing structure of back-streaming electrons and reach the detector. In addition, the scattered deuterons and tritons with energy of about 100 keV can also get to the detector. These particles will be able to pass through the aluminum layer and deposit energy in YAP:Ce. However, the energies deposited by them are very small compared with the energy deposited by the 3.5-MeV alpha from the D–T reaction. Thus, the signal-to-noise ratio is again expected to be excellent when a simple threshold is appropriately applied (see Fig. 3).

In order to quantitatively study the influences from the background radiation, 10^5 events for each radiation type were simulated. For each radiation, the energy deposited in the scintillator was recorded, and their distributions are shown in Fig. 3. It clearly shows the separation between gammas, electrons, deuterons, tritons and alphas. For 14 MeV neutrons, there are a few events which deposit nearly the same amount of energy compared with 3.5-MeV alphas. Even so, its counting rate is about 10^5 times

Table 5
Number of scintillation photons and photoelectrons recorded entering different components of the detector for detecting 3.5-MeV alphas.

Name of detector component	Numbers of scintillation photons and photoelectrons with uncertainties		
	Without grease	With grease	Directly grown
YAP:Ce	$15{,}708 \pm 272$	$15{,}720 \pm 224$	$15{,}710 \pm 305$
Faceplate	$2031 \pm 119 = \{704 \pm 49^{a} + 1327 \pm 108^{b}\}$	$5038 \pm 400 = \{714 \pm 49^{a} + 4324 \pm 397^{b}\}$	$6343 \pm 492 = \{718 \pm 48^{a} + 5625 \pm 490^{b}\}$
PMT window	1380 ± 317	2023 ± 554	2040 ± 554
Photoelectrons	$243 \pm 63 = \{101 \pm 21^{a} + 142 \pm 44^{b}\}$	$337 \pm 101 = \{102 \pm 22^{a} + 235 \pm 83^{b}\}$	$340 \pm 83 = \{103 \pm 21^{a} + 237 \pm 82^{b}\}$

[a] The number of collimated scintillation photons or photoelectrons.
[b] The number of uncollimated scintillation photons or photoelectrons.

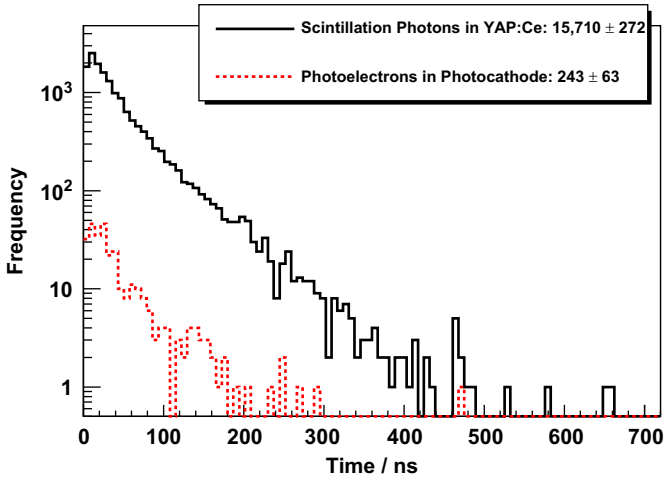

Fig. 2. Time distribution of scintillation photons in the YAP:Ce and time distribution of photoelectrons in the photocathode of PSPMT for detecting 3.5-MeV alpha in the case of no grease between YAP:Ce and faceplate.

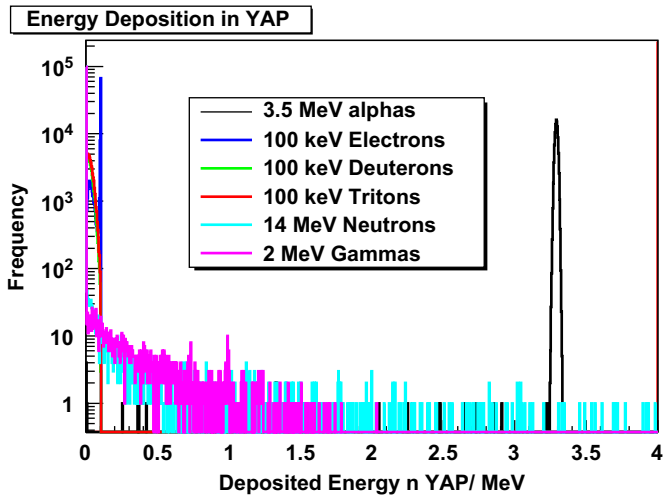

Fig. 3. Distribution of deposited energies of 3.5-MeV alphas, 14-MeV neutrons, 2-MeV gammas, 100-keV electrons, deuterons and tritons.

lower compared with the counting rate of the alpha particles. Since the alpha and 14-MeV neutron are coincident, coincident events between two 14-MeV neutrons are not expected in the event that a 14-MeV neutron triggers the YAP detector.

3.2. Scintillation photon transportation

In order to quantitatively study the loss of scintillation photons in different parts of the detector, code was developed to score the number of optical photons at each interface. In addition, in order to better understand the significance of the presence of the optical coupling compound (at the scintillation–faceplate interface) upon light collection efficiency, two configurations, with and without optical coupling compound at the interface, were studied. In addition, the case in which YAP:Ce is directly grown on the faceplate was also studied. The results are listed in Table 5. Simulation predicts that significant light loss occurs at the interface of the scintillator and the faceplate regardless of the presence of optical grease or the directly-grown YAP:Ce on the faceplate. Without optical grease, 87.1% of the scintillation light will be lost at this interface. This is due to the mismatch of the refractive indexes of the scintillator, vacuum gap, and the faceplate materials. Although optical coupling compound would increase the light collection efficiency at the interface of YAP:Ce and faceplate from 12.9% to 32.0%, it is not possible to include such organic coupling due to the nature of the fabrication process (refer to Section 2.1). Even so, the simulation results suggest that the optical grease would not substantially increase the number of photoelectrons produced at the photocathode. The simulation shows that the numbers of photoelectrons at the photocathode are 243 (2.2% without grease) and 337 (3.4% with grease). Although the total numbers of photoelectrons are different, the numbers of photoelectrons produced by the collimated photons are almost the same for both cases. There are 101 photons produced without grease, and there are 102 photons produced with use of grease. Referring to Table 5, it is also important to note that upon entrance to the fiber-optic faceplate, the number of collimated photons is nearly the same with or without optical grease present.

In addition, since the optical coupling is not possible in the application, the case which YAP:Ce is directly grown on the faceplate was also simulated. From Table 5, it can be seen that the light collection efficiency at the interface between YAP:Ce and faceplate is higher (10.2%) than when coupling grease is present. That is because that the directly-grown case increases the critical angle from 49.9° to 56.4° at this interface, compared with the case where the optical coupling compound is present. But, because of the very small acceptance angle (35.6°) caused by the limited sensitive area of the detector, these increased photons still cannot get to the photocathode in order to increase the number of recorded photoelectrons (see Table 5).

In order to physically understand the results shown in Table 5, a visualization of optical photon transport for the cases of with- and without-optical grease is shown in Fig. 4. Fig. 4b clearly shows that almost all of the uncollimated photons will not be able to make it to the photocathode directly. In the full-sized detector, the diameter of faceplate is 71 mm, and its absorption length at the wavelength of 375 nm is 495 mm, so the tracks of the uncollimated photons which have very large angle relative to the direction of the incident alpha particle still have a chance to be able to get into the light guide and ultimately reach the photocathode to produce photoelectrons. But for the detector that uses the faceplate consisting of 10-μm fibers, it is not possible to build its whole size in the program running on a 16-GB-RAM computer due to the huge number of fibers. In order to

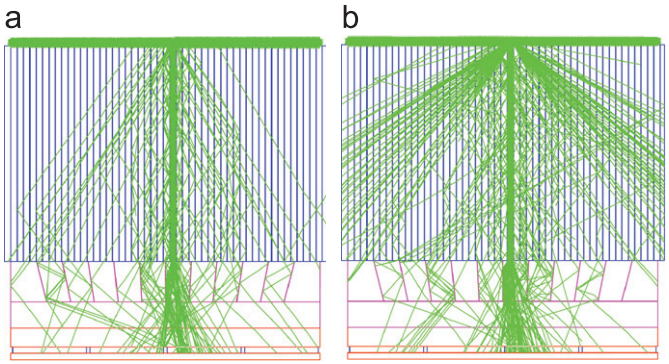

Fig. 4. Visualization of photon propagation in the detector with and without optical grease between the scintillator and the faceplate.

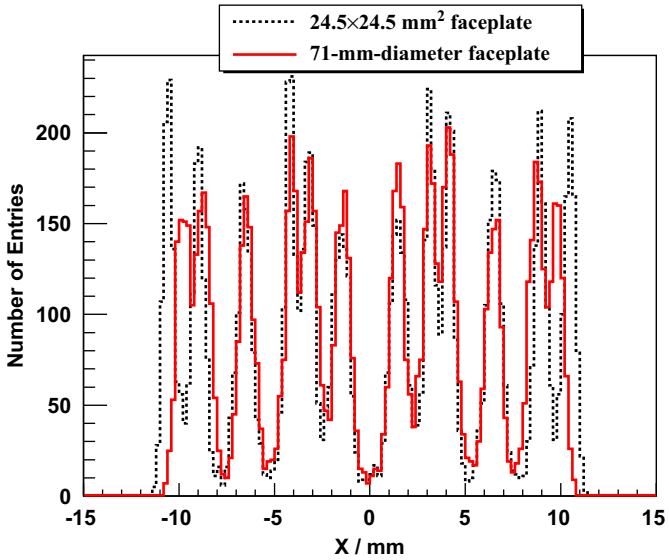

Fig. 5. Projections of flood field response of the detector with different-sized faceplate.

study the influence to the detector performance caused by multi-scattering photons, a detector with a full-sized faceplate having a diameter of 71 mm and consisting of 100-μm fibers was modeled. The projections of the flood field for the detector with the different-sized faceplate are shown in Fig. 5. (The reader is referred to Section 3.3 for a discussion of reconstructing the incident alpha positions.) Compared to the detector with the faceplate size of $24.5\times 24.5\ mm^2$, the full-sized detector can produce more photoelectrons (300 ± 42 vs. 222 ± 60) due to the contribution of the multi-scattering photons. But from Fig. 5, one can see that the multi-scattering photons reduce the average peak-to-valley ratio from 12.7 to 7.0 and also make the position of peaks move toward the center of the detector. Thus, the multi-scattering photons degrade the position performance of the detector.

3.3. Simulated and measured flood field response

To construct the incident positions of alpha particles and furthermore obtain the flood field response of the detector, a four-corner data reconstruction formula (Pani et al., 1999)

$$X=\frac{(A+B)}{(A+B+C+D)},\quad Y=\frac{(B+D)}{(A+B+C+D)} \tag{1}$$

was used, where X and Y are the reconstructed coordinates in two perpendicular directions of the detection plane; A, B, C, and D are the readout values of the four corners of the detector.

In the experiment, a matrix of resistors is used to divide the charges from the 16 channels of the PSPMT into the 4 readout corners, here named A, B, C, and D. But for simplicity in the simulation, the numbers of photoelectrons shared by the resistor chains are used to substitute for the charges of the output signals. To obtain the numbers of electrons at each of the four corners, a two-dimensional convolution matrix was used. Each value in this matrix is a factor which can be used to convert the photoelectrons relative to a given readout pixel into the number of electrons at each corner.

The detector with different-sized-fiber (500 μm, 300 μm, 100 μm, and 10 μm) faceplates for the case of no grease between the scintillator and the faceplate was simulated. The x-axis projections of their flood fields show that the pixels of the detector are very well separated when the 10-μm-fiber faceplate is used (see Fig. 6). The discussion below only concentrates on the detector with 10-μm-fiber faceplate.

Using Eq. (1), the simulated flood fields and their x-axis projections on the detector with and without optical grease were obtained. In order to validate the simulation results, the corresponding experimental flood fields and their x-axis projections were also measured.

Without grease, both experimental and simulated results (Figs. 7 and 8) show a good separation between neighboring pixels of the light guide across the entire detector. With grease, the detector can still distinguish between the neighboring pixels of the light guide, but compared with the case where no grease is used, the separation becomes worse. In addition, the average peak-to-valley ratios of the measured flood fields for both cases (3.4 for without grease; 2.6 for with grease) are worse than the simulated results (16.6 for without grease; 14.9 for with grease). This is explained due to the multi-scattering of photons in the faceplate, which is not included in the simulation (see Section 3.2 for details). It is also explained in that, during the simulation, the gain uncertainties of pixels of the PMT and the tolerance of resistors used to divide the current into four readout corners are not included. One can anticipate that these factors tend to make the separation between the neighboring pixels worse, further degrading the position performance of the detector. The simulated result does also predict that the peak-to-valley ratio worsens when grease is added (see Fig. 8).

In Fig. 8, the x-axis projections of the experimental flood fields show that the amplitudes of the edge pixels are higher than the ones of the center pixels. While, in the simulation data, they do not show the same tendency. The reason is that in the simulation all events are produced within the sensitive area, but in the experiment, this is not the case. In the experiment, the diameter of the scintillator is two inches, and larger than the sensitive area of the detector. The only part of the scintillation photons (uncollimated photons) produced by the events interacting with outside the sensitive area of the detector are recorded by its edge pixels. Thus, the reconstructed points of these events are going to fall into the ranges of the edge pixels. In addition, these events also broaden the width of individual peak in Fig. 8.

In addition, with grease, the flood image of the detector contracts toward the center about 1 mm in each direction compared with the flood field of the detector without grease between the scintillator and the faceplate. In the center area, the reconstructed positions of the light guide pixels exhibit almost no change. In order to explain these phenomena, events from two particular cases on incidence were visualized. An alpha particle was shot near the edge of the scintillator, either in the case with grease or without grease. It was found that for the case without

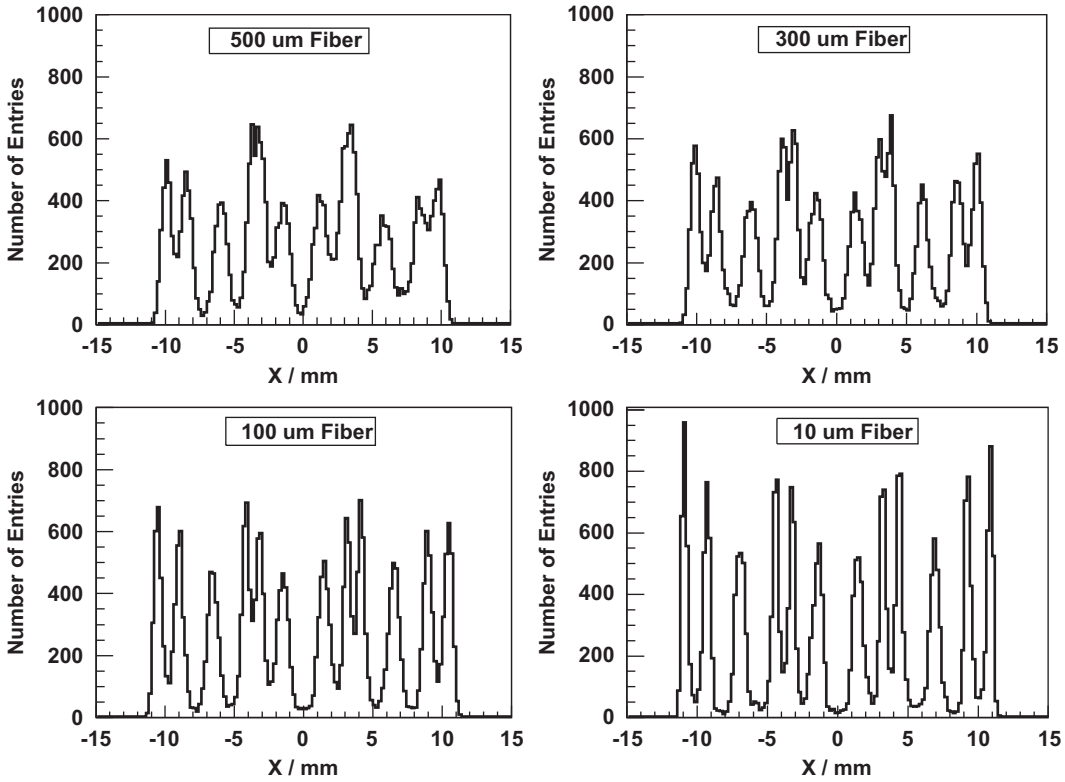

Fig. 6. Projection of flood field response of the detector with four different-sized-fiber faceplates.

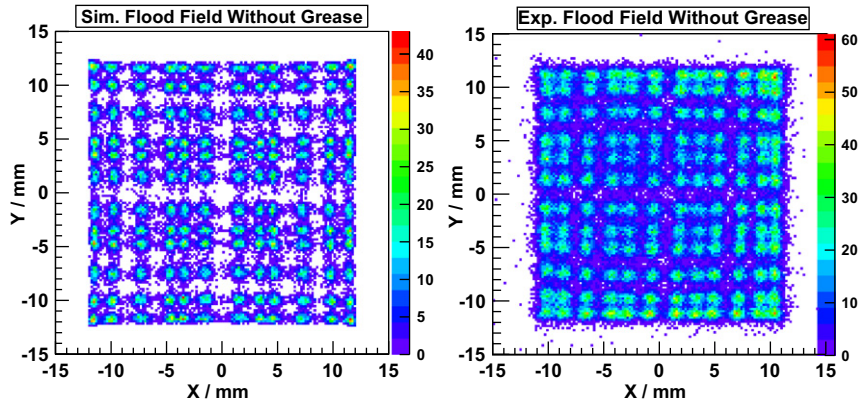

Fig. 7. The simulated and measured flood fields of the detector without grease between the scintillator and the faceplate.

grease, only 3 of 4 PSPMT pixels tend to fire; in the case with grease, all four pixels are often expected to fire. It is generally true that interactions near to edge tend to cause more pixels to fire when optical grease is present. Thus, the reconstructed position with grease is moved more toward the center of the detector compared to the one without grease.

3.4. Position uncertainty

In order to qualitatively study the position performance of the detector, the position deviation was calculated by

$$R_{dev} = \sqrt{(X_{recons} - X_{incid})^2 + (Y_{recons} - Y_{incid})^2}, \quad (2)$$

where X_{recons} and Y_{recons} are the reconstructed positions of alphas; X_{incid} and Y_{incid} are the incident positions of alphas. Fig. 9 shows the distributions of the position deviation for the detector with and without optical grease between the scintillator and the faceplate. The position deviation for the detector with and without grease are about 0.949 ± 1.198 mm and 0.832 ± 0.994 mm, respectively. Here and in Fig. 9, the uncertainty of position deviation is the full width of half maximum. Based upon simulated data, it is expected that the position uncertainty for the detection of 3.5-MeV alphas for the current design without grease is better than 1 mm. In addition, the position performance of the current design for 5.4-MeV alphas was also studied. Its position deviation for the no grease case is 0.812 ± 0.963 mm, slightly better than ones (0.832 ± 0.994 mm) for detecting 3.5-MeV alphas. It can be concluded that the change of energy from 3.5 MeV to 5.4 MeV does not significantly influence the position performance of the detector.

In order to improve its position uncertainty, a Hamamatsu H9500 PSPMT with smaller readout pixels (pixel size: 2.8 mm)

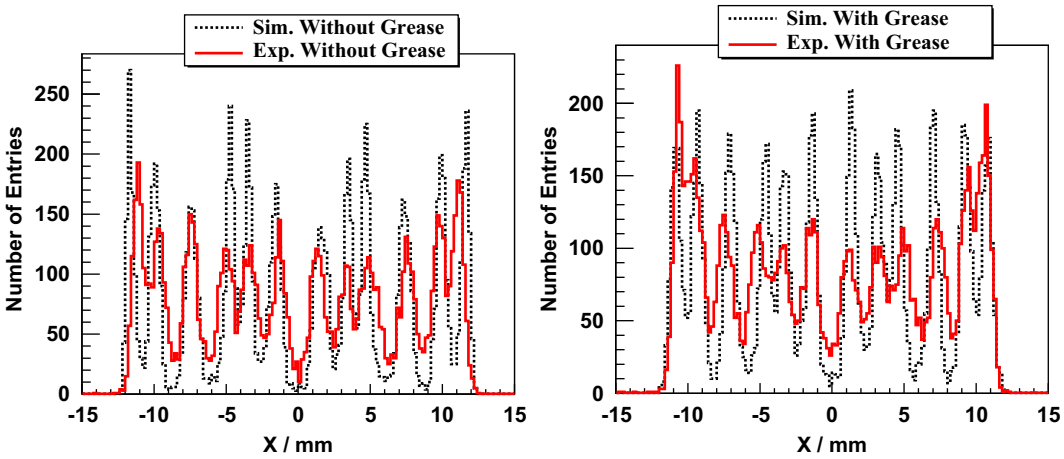

Fig. 8. The *x*-axis projection of simulated and measured flood fields of the detector with and without grease between the scintillator and the faceplate for the same number of events.

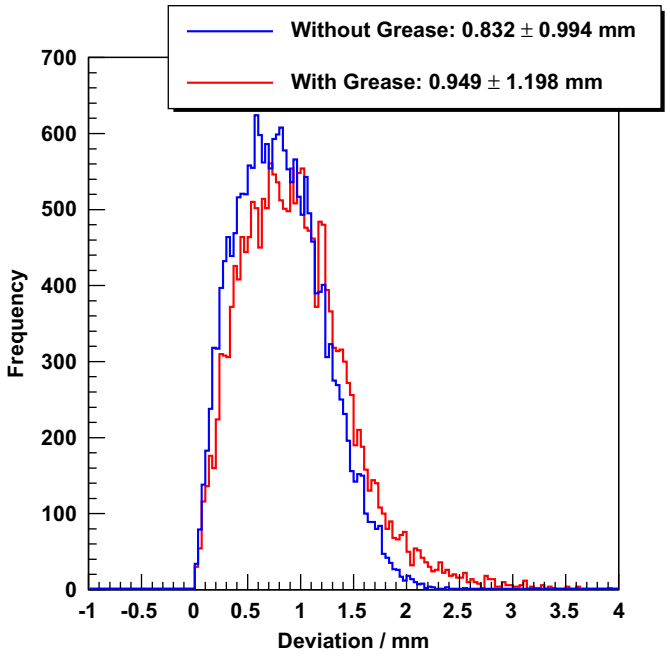

Fig. 9. Distribution of deviation between the incident and reconstructed positions of 3.5-MeV alphas for with and without optical grease between the scintillator and faceplate.

could be used to substitute for the current H8500 (pixel size: 5.8 mm). In this case, it is expected that the pixel size of light guide would need to be smaller than the one used for this design (Blackston et al., 2008).

4. Conclusion

In summary, the performance of an associated alpha-particle detector has been studied in detail with a GEANT4-based full system model. This model includes all relevant physics from the interaction of the incident D–T alphas, to scintillation light creation and transport and photoelectron production. Accounting for some additional variance introduced in the PSPMT design, the simulated flood field shows agreement with the experiment. The agreement is good enough to allow us to use the model to predict expected changes in performance when particular design changes are made. The simulation suggests that 10-μm-fiber faceplate can get best position performance. Although the optical grease between the scintillator and the faceplate will increase the number of photoelectrons, this study suggests that it neither help to improve the quality of flood field of the detector nor its position performance (See Figs. 8 and 9). Less than 1 mm position uncertainty for alpha-particle detector is expected. Additionally, the studies of the detector's response shows that an increase in alpha energy from 3.5 to 5.4 MeV does not significantly influence the position performance of the detector. In addition, the simulation also shows that the thin YAP:Ce and aluminum film used in the current design of associated alpha detector as well as a simple threshold employed during the data taking can minimize the influence of background radiations inside the D–T generator.

Acknowledgements

The authors acknowledge the very helpful discussions and suggestions by Dr. Matthew A. Blackston when the GEANT4-based simulation program was being developed. The authors also would like to thank Dr. M. Nance Ericson for fabrication of the readout boards for the H8500 PSPMT.

References

Agostinelli, S., Allison, J., et al., 2003. Geant4—a simulation toolkit. Nucl. Instrum. Methods A 506, 250–303.
Baccaro, S., Blaek, K., de Notaristefani, F., Maly, P., Mares, J., Pani, R., Pellegrini, R., Soluri, A., 1995. Scintillation properties of YAP:Ce. Nucl. Instrum. Methods A 361, 209–215.
Baccaro, S., Cecilia, A., Montecchi, M., Malatesta, T., de Notaristefani, F., Torrioli, S., Vittori, F., 1998. Refractive index and absorption length of YAP:Ce scintillation crystal and reflectance of the coating used in YAP:Ce single-crystal matrix. Nucl. Instrum. Methods A 406, 479–485.
Blackston, M.A., Habte, F., Hausladen, P.A., 2008. A comparison of geant4 and detect2000 for the simulation of light transport in scintillation detectors. In: Nuclear Science Symposium Conference Record, 2008, NSS '08. IEEE, pp. 4995–4998.
Bourret-Courchesne, E., Derenzo, S., Weber, M., 2009. Development of ZnO: Ga as an ultra-fast scintillator. Nucl. Instrum. Methods A 601, 358–363.
Cates, J., Hayward, J., Zhang, X., Hausladen, P., Dabbs, B., 2011. Timing resolution study of an associated particle detector for fast neutron imaging. IEEE Trans. Nucl. Sci., accepted (No. TNS-00754-2011.R1).
Chichester, D., Lemchak, M., Simpson, J., 2005. The API 120: a portable neutron generator for the associated particle technique. Nucl. Instrum. Methods B 241, 753–758.
Cooper, J.C., Koltick, D.S., Mihalczo, J.T., Neal, J.S., 2003. Evaluation of ZnO(Ga) coatings as alpha particle transducers within a neutron generator. Nucl. Instrum. Methods A 505, 498–501.
Derenzo, S., Weber, J., Moses, W., Dujardin, C., 2000. Measurements of the intrinsic rise times of common inorganic scintillators. IEEE Trans. Nucl. Sci., 860–864.

Hausladen, P., Bingham, P., Neal, J., Mullens, J., Mihalczo, J., 2007. Portable fast-neutron radiography with the nuclear materials identification system for fissile material transfers. Nucl. Instrum. Methods B 261, 387–390.

Hausladen, P., Neal, J., Mihalczo, J., 2005. An alpha particle detector for a portable neutron generator for the Nuclear Materials Identification System (NMIS). Nucl. Instrum. Methods B 241, 835–838.

Kapusta, M., Balcerzyk, M., Moszynski, M., Pawelke, J., 1999. A high-energy resolution observed from a YAP:Ce scintillator. Nucl. Instrum. Methods A 421, 610–613.

Moszynski, M., Kapusta, M., Mayhugh, M., Wolski, D., Flyckt, S., 1997. Absolute light output of scintillators. IEEE Trans. Nucl. Sci. 44, 1052–1061.

Motta, D., Schnert, S., 2005. Optical properties of bialkali photocathodes. Nucl. Instrum. Methods A 539, 217–235.

Neal, J., Giles, N., Yang, X., Wall, R., Ucer, K., Williams, R., Wisniewski, D., Boatner, L., Rengarajan, V., Nause, J., Nemeth, B., 2008. Evaluation of melt-grown, ZnO single crystals for use as alpha-particle detectors. IEEE Trans. Nucl. Sci. 55, 1397–1403.

Nebbia, G., Lunardon, M., Moretto, S., Pesente, S., Viesti, G., Fontana, A., Zenoni, A., Cinausero, M., Nad, K., Obodhas, J., Sudac, D., Valkovic, V., Matika, D., 2005. The use of tagged 14 MeV neutron beams for the detection of illicit materials in land and sea transportation. In: Nuclear Science Symposium Conference Record, 2005. IEEE, pp. 134–137.

Pani, R., Soluri, A., Scafe, R., Pergola, A., Pellegrini, R., 1999. De Vincentis, 1999. Multi-PSPMT scintillation camera. IEEE Trans. Nucl. Sci. 46, 702–708.

Perot, B., Carasco, C., et al., 2007. Development of the EURITRACK tagged neutron inspection system. Nucl. Instrum. Methods B 261, 295–298.

Perot, B., Carasco, C., Mariani, A., Ma, J.L., Dejoies, S., El Kanawati, W., Eleon, C., 2009. Applications of the associated particle technique. In: 2009 First International Conference on Advancements in Nuclear Instrumentation Measurement Methods and their Applications (ANIMMA), pp. 1–7.

Pesente, S., Nebbia, G., Viesti, G., Daniele, F., Fabris, D., Lunardon, M., Moretto, S., Nad, K., Sudac, D., Valkovic, V., 2007. Progress in tagged neutron beams for cargo inspections. Nucl. Instrum. Methods B 261, 268–271.

Rakic, A., 1995. Algorithm for the determination of intrinsic optical constants of metal films: application to aluminum. Appl. Opt. 34, 4755–4767.

Zorenko, Y., Gorbenko, V., Konstankevych, I., Voznjak, T., Savchyn, V., Nikl, M., Mares, J., Nejezchleb, K., Mikhailin, V., Kolobanov, V., Spassky, D., 2007. Peculiarities of luminescence and scintillation properties of YAP:Ce and LuAP:Ce single crystals and single crystalline films. Radiat. Meas. 42, 528–532.